Journal of Power Sources 195 (2010) 2950–2955

Contents lists available at ScienceDirect

Journal of Power Sources

journal homepage: www.elsevier.com/locate/jpowsour

Short communication

Ordered CoO/CMK-3 nanocomposites as the anode materials for lithium-ion batteries

Haijiao Zhang[a,b], Haihua Tao[b], Yong Jiang[b], Zheng Jiao[a,b], Minghong Wu[b], Bing Zhao[b,*]

[a] Institute of Nanochemistry and Nanobiology, Shanghai University, Shanghai 200444, PR China
[b] Shanghai Applied Radiation Institute, School of Environmental and Chemical Engineering, Shanghai University, Shangda Road 99, Shanghai 200444, PR China

ARTICLE INFO

Article history:
Received 8 July 2009
Received in revised form 14 October 2009
Accepted 2 November 2009
Available online 6 November 2009

Keywords:
Cobalt monoxide
Mesoporous carbon
Anode materials
Lithium-ion batteries

ABSTRACT

A novel ordered mesoporous carbon hybrid composite, CoO/CMK-3, is prepared by an infusing method using $Co(NO_3)_2{\cdot}6H_2O$ as the cobalt source. The products are characterized by X-ray diffraction, transmission electron microscopy and N_2 adsorption–desorption analysis techniques. It is observed that the CoO nanoparticles are loaded in the channels of mesoporous carbon. The mesopore structure of CMK-3 is destroyed gradually with increasing of the CoO content. The electrochemical properties of samples as the anode materials for lithium-ion batteries are studied by galvanostatic method. The results show that the CoO/CMK-3 composites have higher reversible capacities (more than 700 mAh g^{-1}) and better cycle performance in comparison with the pure mesoporous carbon (CMK-3). Based on the above results, a mechanism is proposed to explain the reason of such a substantial improvement of electrochemical performance in the CoO/CMK-3 composites.

1. Introduction

Because of the wide application in mobile communication devices, portable electronic devices, electrical/hybrid vehicles and miscellaneous power devices, the advanced Li-ion batteries (LIBs) with higher energy capacity and longer cycle lifetime have great demand world widely. Traditional highly graphitized carbon anode materials show low Li storage capacity (<372 mAh g^{-1}) due to LiC_6 formation [1]. In order to get higher capacity, many new carbon-based materials have been investigated, especially amorphous carbon materials, which show enhanced storage capacities (400–700 mAh g^{-1}) compared with those of graphite [2–5]. The excessive storage capacity beyond theoretical value of LiC_6 is thought to be caused by the additional Li-ion storage site at inner micropore, which was formed by defect in the amorphous carbon. However, the Li-ion storage sites are easy to collapse during the charge/discharge process, which leads to the fast fading of specific capacity of the amorphous carbon [6,7]. Moreover, the amorphous carbon materials usually have large surface areas, where the solid electrolyte interface (SEI) films form during the first discharging process to make large irreversible capacity [8,9]. Therefore, in order to improve the electrochemical performance, the structure and the components of the amorphous carbon materials should be devised and synthesized elaborately.

Recently, ordered mesoporous carbon (CMK-3) has been considered as possible nanomaterials with high Li-ion storage capacity. The ordered mesochannel and large surface area of CMK-3 shorten the distance of Li-ion diffusing and its high conductivity is in favor of transmitting the electron [10]. CMK-3 materials were also used to functionalize other materials, improving the electrical conductivity, mechanical and thermal properties [11–13]. Zhou et al. synthesized a mesoporous carbon material by using the mesoporous silica as hard template. The first discharge capacity of the mesoporous carbon material was 3100 mAh g^{-1}, about eight times higher than the theoretical value of LiC_6 [14]. However, the initial coulombic efficiency was only about 34%. Li-ion storage capacity of almost 2000 mAh g^{-1} was irreversible, which attributed to the formation of SEI films on the large surface area. Moreover, the material showed unsatisfactory capacity retention with cycling. Zhao et al. loaded SnO_2 in the mesochannels of CMK-3 by an infusing method [15]. Although the first cycle coulombic efficiency of this composite was improved, the first discharge capacity was only about 520 mAh g^{-1}, and the capacity dropped to about 249 mAh g^{-1} after 20th cycle, only about 60% of the original capacity, compared with the second discharge capacity, about 420 mAh g^{-1}.

CoO is a new type anodic material of lithium-ion batteries with high reversible specific capacity [16,17]. The Li-ion insertion–extraction mechanism and electrochemical performance of various nano-structured CoO materials have been intensively investigated. In this paper we reported a CoO-loaded mesoporous carbon materials, which shows higher reversible capacity, higher coulombic efficiency, and better capacity retention compared with

* Corresponding author. Tel.: +86 21 6613 7501; fax: +86 21 6613 5275.
E-mail address: bzhao@shu.edu.cn (B. Zhao).

0378-7753/$ – see front matter © 2009 Elsevier B.V. All rights reserved.
doi:10.1016/j.jpowsour.2009.11.003

the pure CMK-3. The morphology and structure of CoO/CMK-3 composites were characterized and the electrochemical performances of the composites were investigated. On the basis of the experiment results, a possible mechanism for improved electrochemical properties of CoO/CMK-3 composites was discussed in detail.

2. Experimental

2.1. Synthesis of SBA-15 and CMK-3

According to the method reported by Zhao et al. [18], SBA-15 mesoporous silica materials were synthesized using the triblock copolymer (Pluronic $P_{123,}$ $EO_{20}PO_{70}EO_{20}$, M_{av} = 5800) as the surfactant and tetraethylorthosilicate (TEOS) as the silica source. CMK-3 was similar to the synthesis method described by Ryoo et al. [10]. In a typical synthesis, 1 g of above prepared SBA-15 was added to a solution containing 1.25 g of sucrose, 0.14 g of H_2SO_4 and 5 g of H_2O. The mixture was then put in a drying oven for 6 h at 373 K, and subsequently the temperature of oven was increased to 433 K, then maintained there for another 6 h. After the present step, the sample was treated again at 373 and 433 K using the same drying oven after the addition of 0.8 g of sucrose, 0.09 g of H_2SO_4 and 5 g of H_2O. The carbonization was complemented by pyrolysis with heating to 1173 K under a nitrogen gas protection. The silica template was removed using 5 wt% HF aqueous solutions at room temperature. CMK-3 was obtained after washing with distilled water and drying at 353 K.

2.2. Synthesis of CoO/CMK-3

CoO/CMK-3 composites were prepared by the following steps: 0.6 g CMK-3 was added in a flask-2-neck, and then the flask-2-neck was vacuumized. 15 mL ethanol solution containing a certain amount of $Co(NO_3)_2{\cdot}6H_2O$ was added into the flask. For example, if the target product with CoO mass load of 10 wt%, 0.25 g $Co(NO_3)_2{\cdot}6H_2O$ was added. The above mixture was stirred for 1 h at room temperature under vacuum to make the CMK-3 dispersed completely in the solution. The ethanol was vaporized slowly at 333 K under stirring, and the CoO/CMK-3 composites were obtained after heating the mixture in a tube furnace at 773 K for 4 h under flowing nitrogen. By these procedures we prepared five types of CoO/CMK-3 composites with different CoO contents: 5, 10, 15, 20 and 25 wt%, respectively. The CoO contents were calculated based on the amount of carbon and cobalt precursors. After synthesizing the CoO/CMK-3 composites, the loading CoO amount of the samples was determined by the TG analysis. The testing data were consistent with designed CoO content.

2.3. Characterizations

X-ray powder diffraction (XRD) patterns were obtained on the Japan Rigakul D/max-2550 instrument operating at 40 kV and 40 mA using CuK_α radiation (λ = 0.154 nm). The scanning range 2θ of the wide-angle and low-angle are from 10° to 80° and from 0.5° to 5° respectively, with a step size of 0.02°. The structural properties and morphology of CoO/CMK-3 were studied by a JEOL 200CX, transmission electron microscopy (TEM). N_2 adsorption–desorption isotherms were recorded on a Micromeritics ASAP 2020 at 77 K after evacuation at 573 K for 5 h. Thermal analysis was carried out on a Metter Toledo TGA/SDTA 851^e thermal analyzer with 8–10 mg sample for each measurement. The temperature rise rate was 10 K min^{-1} from room temperature to 1073 K in the flow of air at a flow rate of 30 ml min^{-1}.

For electrochemical measurements, the active materials were mixed and rolled with 10 wt% polytetrafluoroethylene powder to form a film. The obtained film was pressed onto a copper mesh, and dried under vacuum for 10 h at 80 °C. The electrolyte used was 1 M $LiPF_6$ dissolved in dimethyl carbonate (DMC), diethyl carbonate (DEC) and ethylene carbonate (EC) (1:1:1 by weight). Lithium metal was used as the counter electrode. The cell was assembled in a glove box filled with argon gas. Each cell contained about 3.6 mg active materials. Discharge/charge testing was carried out on Land-CT2001A battery test system with a constant discharge/charge rate at 100 mAg^{-1}.

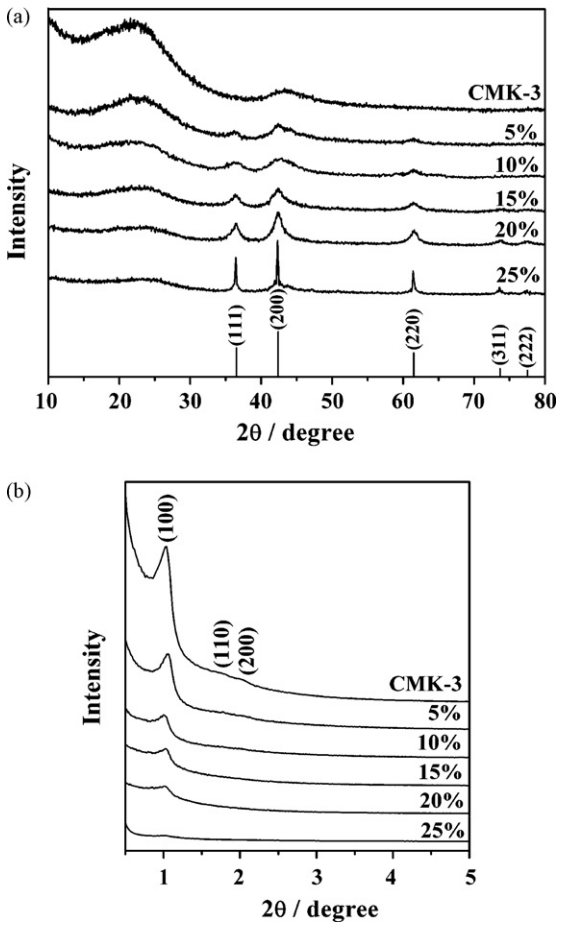

Fig. 1. X-ray diffraction patterns of CoO/CMK-3 composites with different CoO contents: (a) wide-angle and (b) low-angle.

3. Results and discussion

Fig. 1 shows the wide-angle and low-angle XRD patterns of CoO/CMK-3 composites with different CoO contents. In Fig. 1(a), the two broad diffraction peaks (0 0 2) and (1 0 0) of the graphite structure were observed in the wide-angle XRD pattern of CMK-3, which indicates that the CMK-3 is not highly graphitized. After loading CoO, five diffraction peaks appear in Fig. 1(a) at 2θ = 36.5°, 42.4°, 61.5°, 73.7°, 77.5°, respectively, which can be indexed to cubic structure of CoO for the planes of (1 1 1), (2 0 0), (2 2 0), (3 1 1), (2 2 2) (PDF No. 43-1004). With the increasing of CoO content, the intensity of diffraction peaks increases gradually and becomes sharper, which indicates that increasing the content of $Co(NO_3)_2{\cdot}6H_2O$ in the precursors not only increases the quantity of CoO in the sample, but also leads to enlarge the diameter of CoO nanoparticles. As can be seen in Fig. 1(b), an intense peak (1 0 0) and two weaker peaks (1 1 0) and (2 0 0) are observed in the low-angle XRD patterns of CMK-3, which associates with the 2-d hexagonal mesostructure with *P6 m* space group [10]. With increasing of loading CoO amount, the intensity of these peaks gradually decreases. The (1 0 0) peak of

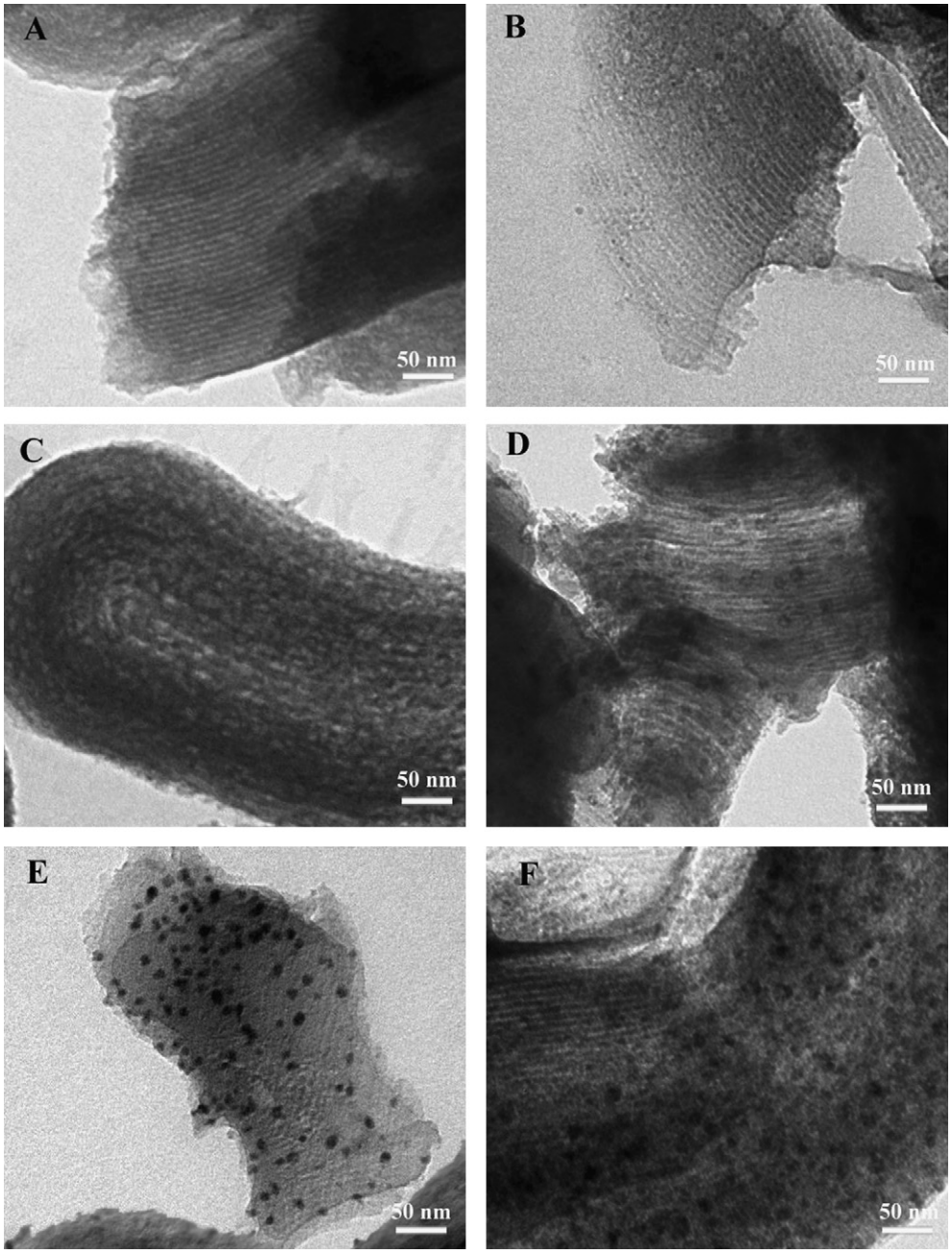

Fig. 2. TEM images of CoO/CMK-3 composites with different CoO contents: (A) CMK-3 without loading and loading with CoO, (B) 5 wt%, (C) 10 wt%, (D) 15 wt%, (E) 20 wt%, and (F) 25 wt%.

the CMK-3 is almost not observed in 25 wt% CoO-loaded sample, which indicates that most of the ordered structure was destroyed during the loading process in this heavy CoO-loaded sample. The similar phenomenon has been observed previously [19].

Fig. 2 shows the TEM images of CoO/CMK-3 composites with different CoO contents. The mesopore structure of CMK-3 can be clearly observed in the TEM images. The CoO nanoparticles uniformly dispersed inside the CMK-3 framework. With the CoO content increasing, the size of CoO nanoparticles increases gradually. The average CoO particle sizes of various composites which are estimated from TEM images are listed in Table 1. When the loading amount is over 20 wt%, the average CoO particle size becomes more than 10 nm, much larger than the mesopore diameter of CMK-3 (3.7 nm). The large CoO nanoparticles may destroy the mesopore structure of CMK-3 and decrease the ordered level of 2-D hexagonal mesostructure of CMK-3 framework, which is consistent with the XRD results.

The N_2 adsorption–desorption isotherms of pure CMK-3 and CoO/CMK-3 composites with different CoO contents are shown in Fig. 3. All the samples exhibit typical type IV isotherms with a H_1 hysteresis loop which are typical adsorption for mesoporous materials with 2-D hexagonal ordered structure [10]. The pronounced capillary condensation steps confirm the mesoporous structure of the hybrid composites. As listed in Table 1, the textural properties of the CoO/CMK-3 composites systematically decrease with the increasing of amount of CoO, such as BET surface area (from 1168 to 825 $m^2\,g^{-1}$), pore size (from 3.63 to 2.67 nm) and pore volume (from 1.06 to 0.55 $cm^3\,g^{-1}$), which affirm CoO grown inside the mesochannels of the CMK-3. In order to deduct the impact of the weight of loading CoO on textural properties such as surface

Table 1
Textural properties of CoO/CMK-3 composites with different CoO contents.

CoO content (wt%)	S_{BET}[a] ($m^2\ g^{-1}$)	Pore size[b] (nm)	Pore volume[c] ($cm^3\ g^{-1}$)	Size of CoO[d] (nm)	Absolute surface area of CMK-3 ($m^2\ g^{-1}$)[e]	Absolute pore volume of CMK-3 ($cm^3\ g^{-1}$)[f]
0	1168	3.63	1.06	–	–	–
5	1067	3.64	0.97	3.5	1123	1.03
10	1030	3.60	0.85	3.9	1144	0.96
15	1000	3.04	0.76	7.8	1176	0.92
20	922	2.86	0.66	9.3	1153	0.86
25	825	2.67	0.55	12.5	1100	0.79

[a] Surface area calculated by the (Brunauer–Emmett–Teller) BET method.
[b] Adsorption average pore width (4 V/A by BET).
[c] Total pore volume measured at $p/p_0 = 0.96$.
[d] The size of CoO estimated from TEM image.
[e] Absolute surface area of CMK-3 calculated as formula 1.
[f] Absolute pore volume of CMK-3 calculated as formula 2.

area and pore volume, the absolute surface area and the absolute pore volume of the CMK-3 framework of each sample have been calculated as below.

3.1. The absolute surface area of CMK-3

Compared with the surface area of CMK-3, the surface area of CoO is so small that it can be ignored in the calculation. The absolute surface area of CMK-3 can be estimated as the following formula (1):

$$(1 - x)S_{\text{CMK-3}} = S_{\text{m}} \quad (1)$$

$S_{\text{CMK-3}}$ is the absolute surface area of CMK-3; S_{m} is the measured surface area of the sample; and x is the content of CoO.

3.2. The absolute pore volume of CMK-3

The absolute pore volume of CMK-3 is supposed to be composed of two parts: one is the measured pore volume (empty volume) and the other is the volume occupied by loading CoO. So the absolute pore volume of CMK-3 is estimated as the following formula (2):

$$(1 - x)V_{\text{CMK-3}} = V_{\text{m}} + \frac{x}{\rho_{\text{CoO}}} \quad (2)$$

$V_{\text{CMK-3}}$ is the absolute pore volume of CMK-3; V_{m} is the measured pore volume; x is the content of CoO; and ρ_{CoO} is the density of CoO (about 6.45 g cm^{-3}).

The absolute surface area and absolute pore volume of CMK-3 are listed in the 6th and the 7th columns of Table 1. There are

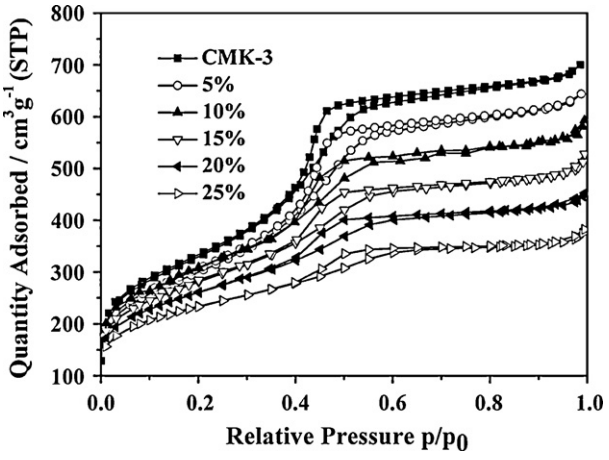

Fig. 3. N_2 adsorption–desorption isotherms of CoO/CMK-3 composites with different CoO contents.

almost no variation of the absolute surface area of CMK-3 framework, which may indicates the channels of CMK-3 are not blocked by loading CoO, or else the absolute surface area of CMK-3 may evidently decreases. However, the absolute pore volume of CMK-3 decreases with increasing the CoO content, which probably indicates that mesopore structure of CMK-3 is partially destroyed by CoO deposition. This result is consistent with the analysis from the pore size and TEM images.

Fig. 4 presents the charge/discharge curves of the CMK-3 with different CoO contents between 0.005 and 3.0 V (vs. Li^+/Li). Large charge/discharge voltage hysteresis between the charge/discharge processes exists and no distinct potential plateaus on the charge/discharge curves, which are similar to other amorphous carbon [20,21]. When the CoO content exceeds 10 wt%, there are only inflexions on the charge/discharge curves appear at the range from 1.4 to 1.0 V and 1.9 to 2.3 V after the first cycle, which correspond to the discharge and charge processes of CoO [16,17]. Fig. 5 compares the charge/discharge capacities and initial coulombic efficiency of all composites with different CoO contents in the first cycle. The pure CMK-3 exhibits a discharge capacity of 1600 mAh g^{-1} and the charge capacity of 520 mAh g^{-1}, corresponding to a coulombic efficiency of 32.5%. With the increase of CoO content, the discharge capacity of the CoO/CMK-3 composites gradually decreases to 1170 mAh g^{-1}. But the charge capacity increases to 710 mAh g^{-1} when CoO content gets to 15 wt%, and then decreases to 560 mAh g^{-1} when CoO content gets to 25 wt%. The irreversible capacity of the first cycle decreases from 1100 mAh g^{-1} of pure CMK-3 to 620 mAh g^{-1} of 25 wt% CoO-loaded composite. The initial coulombic efficiency intensively increases to more than 47% when CoO content exceeds 15 wt%. The irreversible capacity of amorphous carbon materials at the first cycle is mainly attributed to the solid electrolyte interface (SEI) formation and a part of Li-ion inactivation after the first cycle, the degree of which is proportional to the surface area of carbon and the irreversible storage of Li-ions at void or cavity sites [6]. Seen from the analyses of the morphology and structure, there are abundant mesopores in CMK-3, which results in a large surface area about 1168 $m^2\ g^{-1}$. That might be the reason for the large irreversible capacity and low coulombic efficiency of pure CMK-3, just as shown in Scheme 1(a). When CoO particles are loaded in the channel of CMK-3, the surface area of the hybrid composites obviously decrease as shown in Table 1. That might be the major reason for continuing decrease of irreversible capacity of the CoO/CMK-3 composites with increasing CoO content, and also the initial discharge capacity of the CoO/CMK-3 composites continuously decreases with increasing CoO content. The decrease of irreversible capacity with CoO loading induces a notable improvement of the initial coulombic efficiency.

Fig. 6 shows the cycle performance of CoO/CMK-3 composites with different CoO contents. For the pure CMK-3, the capacity is

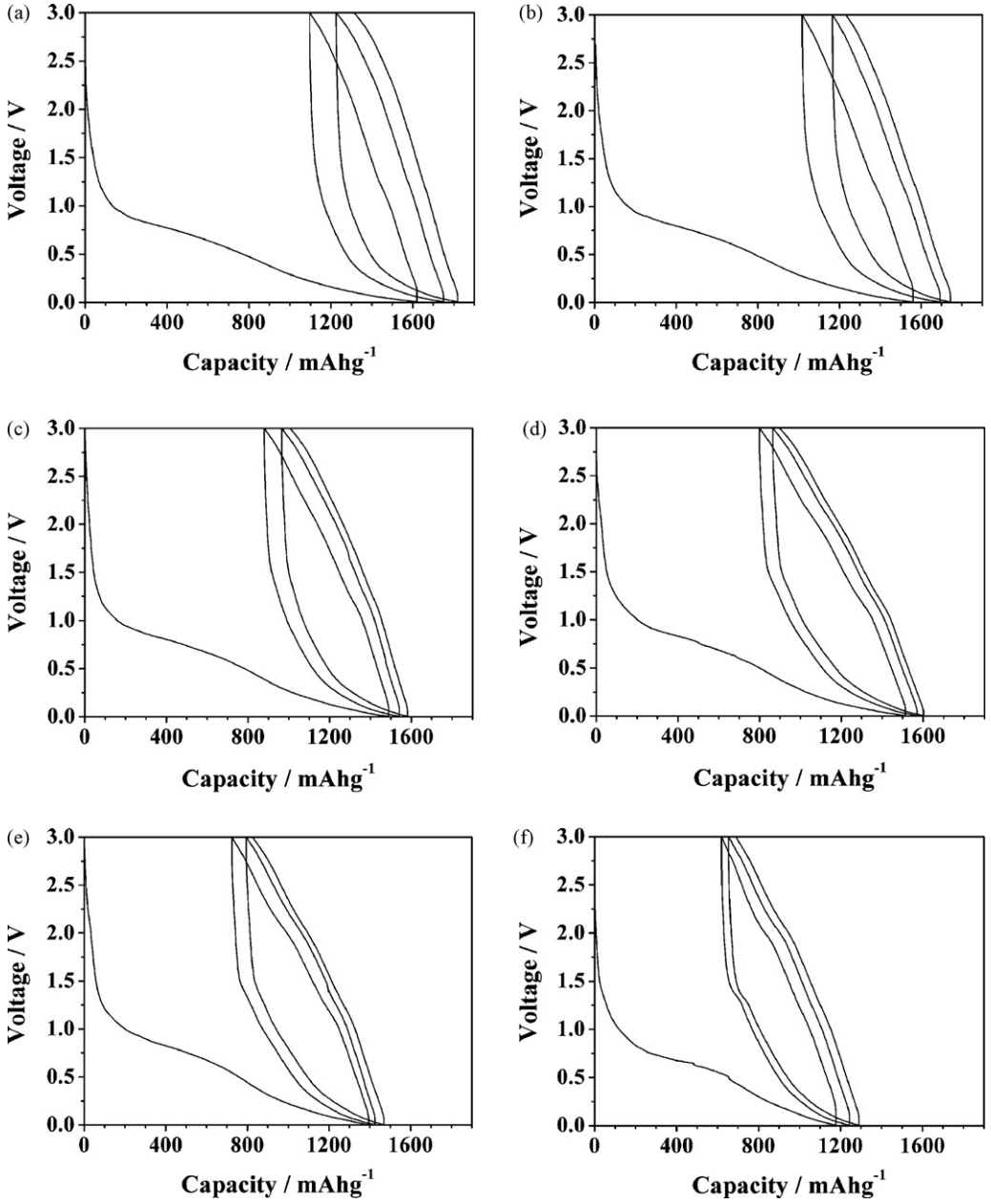

Fig. 4. The first three charge–discharge cycles of the CoO/CMK-3 composites with different CoO contents: (a) CMK-3 without loading and loading with CoO, (b) 5 wt%, (c) 10 wt%, (d) 15 wt%, (e) 20 wt%, and (f) 25 wt% at a current density of 100 mA g^{-1} between 0.005 V and 3.0 V.

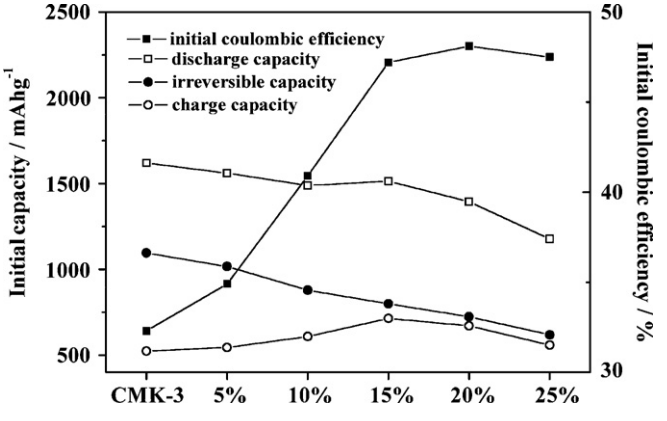

Fig. 5. The initial capacity and coulombic efficiency of CoO/CMK-3 composites with different CoO contents.

about 650 mAh g^{-1} (corresponding to the discharge capacity of the 2nd cycle), which is much higher than the theoretical value of graphitized carbon. However the capacity is only 350 mAh g^{-1} after 20 cycles, just the 61% of the capacity of the 2nd cycle. As previously reported, there are a lot of cavities and micropores in the carbon matrix of CMK-3, and also there are many disordered carbon atoms stacking zones, supplying excess lithium storage positions. However, the structure around these positions is not very stable because the inner force induced from the volume variation during cycling is prone to make the structure destroyed, which makes more and more pores and cavities passivated and loss capacity. That might be the reason for serious capacity decay of CMK-3 at the cycling proceeds. When increasing the CoO content to 15 wt%, the capacity of the samples gradually grows up to about 771 mAh g^{-1}. The 15 wt% CoO-loaded composite also shows the best cycle performance. The capacity is 709 mAh g^{-1} after 20 cycles, about 92% of the discharge capacity of the 2nd cycle. CoO is a good anode material of

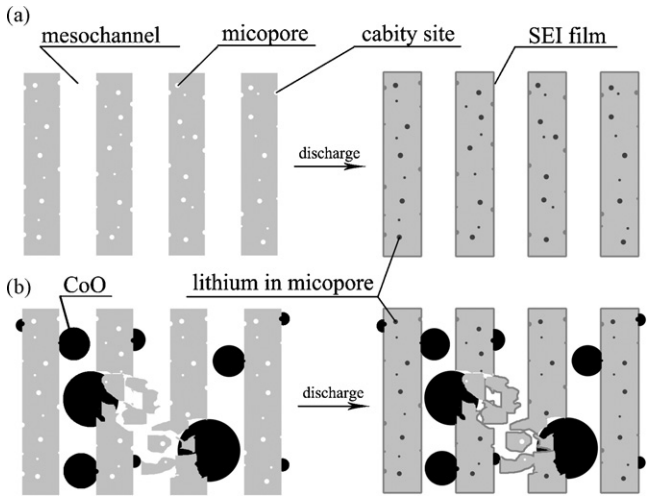

Scheme 1. The first discharge process of (a) CMK-3 and (b) CoO/CMK-3 composites with heavy loading.

Li-ion batteries and its theoretical capacity is about 715.4 mAh g^{-1} [17], which is higher than the capacity value of pure CMK-3 (about 650 mAh g^{-1}) in our experiment. So the hybrid composites with different CoO loading contents show higher capacity than pure CMK-3. However the theoretical capacity of the 15 wt% CoO-loaded sample which calculates from the theoretical capacity of CoO and the capacity of pure CMK-3 is only about 660 mAh g^{-1}, which is lower than its experimental value (about 771 mAh g^{-1}). The reasons for such a high capacity are not very clear now. According to the literature [17], there may be some additional Li-ion reduced and stored in the boundary between Co and Li_2O during the discharge process, which is extracted in the following charge cycle. The intercalation-extraction of the additional Li-ion in the CoO enlarges the capacity of CoO. Then the capacity of CoO can reach to about 1200 mAh g^{-1} [17]. Based on this capacity value, the capacity of the 15 wt% CoO-loaded sample can be about 733 mAh g^{-1}, which is similar to our experimental value. This is a possible explanation for the high capacity of 15 wt% CoO-loaded sample. Furthermore, when the CoO content is less than 15 wt%, the CoO nanoparticles homogeneously disperse in the channels of CMK-3. The mesopore structure prevents CoO from aggregating. The nano-sized CoO closely contacted with carbon matrix ensures a good electrical conductivity. The mesopore channel also provides enough space to buffer the volume change during the Li-ion insertion and extraction reactions in CoO nanoparticles. All of these factors above-mentioned

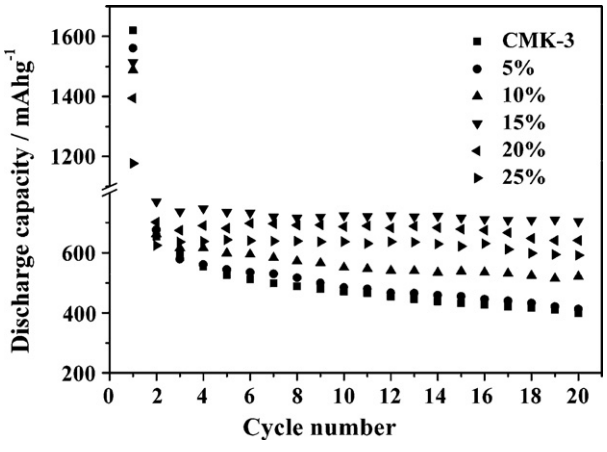

Fig. 6. Cycling performance of CoO/CMK-3 composites with different CoO contents at a current density of 100 mA g^{-1} between 0.005 and 3.0 V.

enhance the cyclability of CoO/CMK-3 composites. When the CoO loading content exceeds 15 wt%, CoO nanoparticles in the mesopore of CMK-3 becomes very large and probably destroy the CMK-3 framework, just as shown in Scheme 1(b). With CoO particle size increasing, the stress and volume change of CoO nanoparticles during Li-ion insertion and extraction reaction may result in decreasing the electrical conductivity between CoO nanoparticles and CMK-3 framework. These may be the reasons for the lowering of the capacity of CoO/CMK-3 with loading amount above 20 wt%.

4. Conclusions

In conclusion, we developed a simple and effective method to synthesize CoO/CMK-3 composites by an infusing method, in which CoO nanoparticles were successfully filled in the ordered channels of CMK-3. The CoO/CMK-3 composites showed better electrochemical performance than the pure CMK-3 including specific capacity, coulombic efficiency and cycling capability. This substantial improvement of electrochemical performance may be attributed to the synergistic effects in the CoO/CMK-3 composites. Loaded CoO nanoparticles reduce the surface area of the CMK-3, which decrease the irreversible capacity and improve the initial coulombic efficiency of the CoO/CMK-3 composites. The homogeneously dispersed CoO nanoparticles keep good electrical conductivity with CMK-3 framework. The mesopore structure of CMK-3 is tolerant to the stress and volume change of CoO nanopaticles during Li-ion insertion and extraction process. These synergistic effects make the CoO/CMK-3 composites higher specific capacity and better cycling performance.

Acknowledgements

The authors thank Dr. Xiang Xu for help with the BET measurements. We gratefully acknowledge financial supports from the MOST 973 Program (2006CB705604), Shanghai Leading Academic Disciplines (S30109), Natural Science Foundation of China (20871081), Natural Science Foundation of Shanghai (08ZR1407800, 09ZR1411800), Innovation Program of Shanghai Municipal Education Commission (09YZ25, 10YZ05) and Excellent Youth Scholars of Higher Education of Shanghai.

References

[1] S. Flandroisa, B. Simonb, Carbon 37 (1999) 165–180.
[2] K.T. Lee, J.C. Lytle, N.S. Ergang, S.M. Oh, A. Stein, Adv. Funct. Mater. 15 (2005) 547–556.
[3] Y. Zhang, F. Zhang, G.D. Li, J.S. Chen, Mater. Lett. 61 (2007) 5209–5212.
[4] Y.S. Hu, P. Adelhelm, B.M. Smarsly, S. Hore, M. Antonietti, J. Maier, Adv. Funct. Mater. 17 (2007) 1873–1878.
[5] J. Hu, H. Li, X.J. Huang, Solid State Ionics 178 (2007) 265–271.
[6] F. Bonino, S. Brutti, P. Reale, B. Scrosati, L. Gherghel, J. Wu, K. Mullen, Adv. Mater. 17 (2005) 743–746.
[7] Z.H. Yi, Y.G. Liang, X.F. Lei, C.W. Wang, J.T. Sun, Mater. Lett. 61 (2007) 4199–4203.
[8] F. Li, Q.Q. Zou, Y.Y. Xia, J. Power Sources 177 (2008) 546–552.
[9] Q. Wang, H. Li, L.Q. Chen, X.J. Huang, Solid State Ionics 152–153 (2002) 43–50.
[10] S. Jun, S.H. Joo, R. Ryoo, M. Kruk, M. Jaroniec, Z. Liu, T. Ohsuna, O. Terasaki, J. Am. Chem. Soc. 122 (2000) 10712–10713.
[11] Y.M. Fang, H.Q. Hu, Catal. Commun. 8 (2007) 817–820.
[12] K.S. Xia, Q.M. Gao, C.D. Wu, S.Q. Song, M.L. Ruan, Carbon 45 (2007) 1989–1996.
[13] J. Roggenbuck, G. Koch, M. Tiemann, Chem. Mater. 18 (2006) 4151–4156.
[14] H.S. Zhou, S.M. Zhu, M. Hibino, I. Honma, M. Ichihara, Adv. Mater. 15 (2003) 2107–2111.
[15] J. Fan, T. Wang, C.Z. Yu, B. Tu, Z.Y. Jiang, D.Y. Zhao, Adv. Mater. 16 (2004) 1432–1436.
[16] J.S. Do, C.H. Weng, J. Power Sources 146 (2005) 482–486.
[17] J.S. Do, C.H. Weng, J. Power Sources 159 (2006) 323–327.
[18] D.Y. Zhao, J.L. Feng, Q.S. Huo, N. Melosh, G.H. Fredrickson, B.F. Chmelka, G.D. Stucky, Science 279 (1998) 548–552.
[19] H.F. Li, H.A. Xi, S.M. Zhu, R.D. Wang, Mater. Lett. 60 (2006) 943–946.
[20] E. Frackowiak, S. Gautier, H. Gaucher, S. Bonnamy, F. Beguin, Carbon 37 (1999) 61–69.
[21] Y.P. Wu, E. Rahm, R. Holze, J. Power Sources 144 (2003) 228–236.